SAE INTERNATIONAL

ARTICLE INFO
Article ID: 03-16-07-0055

doi:10.4271/03-16-07-0055

Thin-Wire Thermocouple Design for Exhaust Gas Temperature Pulse Measurements in Internal Combustion Engines

Varun Venkataraman,[1] Ola Stenlåås,[1,2] and Andreas Cronhjort[1]

[1]KTH Royal Institute of Technology, CCGEx, Department of Engineering Design, Sweden
[2]Scania CV AB, Sweden

Abstract

Accurate exhaust gas temperature (EGT) measurements are vital in the design and development process of internal combustion engines (ICEs). The unsteady ICE exhaust flow and thermal inertia of commonly used sheathed thermocouples and resistance thermometers require high bandwidth EGT pulse measurements for accurate cycle-resolved and mean EGTs. The EGT pulse measurement challenge is typically addressed using exposed thin-wire resistance thermometers or thermocouples. The sensor robustness to response tradeoff limits ICE tests to short durations over a few exhaust conditions. Larger diameter multiwire thermocouples using response compensation potentially overcomes the tradeoff. However, the literature commonly adopts weaker slack wire designs despite indications of coated weld taut wires being robust. This study experimentally evaluates the thin-wire thermocouple design placed in the exhaust of a heavy-duty diesel engine over wide-ranging exhaust conditions for improving both sensor robustness and accuracy of the measured EGT. The assessed design parameters included the wire diameter (51 μm to 254 μm), the exposed wire length, and the wires placed slack or taut with coated weld faces. All taut wires with ceramic-coated weld faces endured over 3 h of engine operation, while similar diameter slack wires (51 μm and 76 μm) were sensitive to the exhaust condition and exposed wire length. Reducing the wire diameter from 76 μm to 51 μm significantly impacted response improvements as evidenced at certain test conditions by a peak-peak EGT increase of 92 °C, a mean EGT drop of 26 °C, and a doubling of the sensitivity of mean EGT cycle-to-cycle variations to ±12 °C. Increasing the exposed wire length showed less significant response improvements. The Type-K thin-wire thermocouples showed negligible drift, thereby indicating the possibility of using smaller and longer wires built taut with coated weld faces for improved accuracy of EGT measurements in ICEs.

History

Received: 24 Nov 2022
Revised: 14 Feb 2023
Accepted: 28 Apr 2023
e-Available: 17 May 2023

Keywords

Pulsating flow, Crank-resolved measurement, Time-resolved measurement, Test equipment and instrumentation, Bare-wire, fine-wire, fine-gauge thermocouples, Gas thermometry, Sensor/probe fabrication, Ceramic coatings, Sensor robustness, Multiwire thermocouples

Citation

Venkataraman, V., Stenlåås, O., and Cronhjort, A., "Thin-Wire Thermocouple Design for Exhaust Gas Temperature Pulse Measurements in Internal Combustion Engines," *SAE Int. J. Engines* 16(7):987-1005, 2023, doi:10.4271/03-16-07-0055.

ISSN: 1946-3936
e-ISSN: 1946-3944

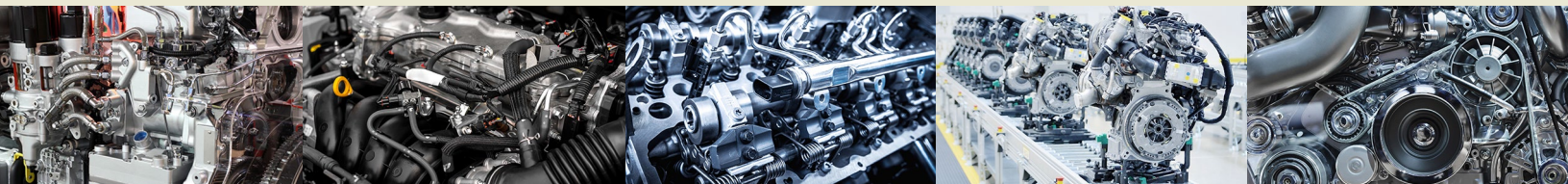

Introduction

The exhaust gas temperature (EGT) is a crucial parameter for assessing the efficiency and optimization of turbocharging and exhaust aftertreatment (EAT) systems impacting both the performance and emissions in internal combustion engines (ICEs). EGT measurements are typically performed using sheathed invasive thermal sensors such as thermocouples and resistance thermometers to represent the mean EGT. However, the measured mean temperature differs from the true EGT due to the thermal inertia and heat balance of the sensor, which needs to be addressed by sensor design or compensated with additional measurements. When considering measurement locations pre-turbine or in the exhaust of single-cylinder (research) engines, the pulsating flow is highly unsteady with large amplitude EGT fluctuations over short timescales. Sheathed invasive thermal sensors do not capture the high-frequency content in EGT pulses.

Conventionally, one-dimensional gas dynamic system simulations are used to estimate the rapid EGT fluctuation in ICEs. The model validation utilizes high bandwidth piezoresistive pressure sensors to compare the associated pressure-based gas dynamics. However, EGT validation is limited to invasive sheathed thermal sensors that only provide a mean temperature reference [1]. EGT pulse measurements have been used to assess the unsteady on-engine turbine efficiency [2], estimate exhaust gas pulse energy [3], and validate models for instantaneous heat transfer at the exhaust port [4] alongside early solvers for gas exchange simulations [5]. Additionally, flow unsteadiness with large amplitude fluctuations in the gas temperature and heat transfer coefficient induces a displacement in the mean temperature measured by invasive thermal sensors [6], which may be overcome with high bandwidth EGT measurements [2]. Therefore, resolving the EGT pulse is important to obtain both accurate mean and cycle-resolved EGTs in ICEs. Unlike the widely adopted piezoresistive pressure sensors, the measurement challenges associated with the EGT pulse typically limit its assessment to gas dynamic system models.

A review by Childs et al. [7] on temperature measurement techniques highlights the challenge of simultaneously satisfying high-frequency response requirements over a reasonably high-temperature range (~1000°C) with commercial availability at a low relative cost. Measurement techniques based on laser diagnostics and radiation thermometry are used for in-cylinder gas temperature measurements [8] and can be utilized in the exhaust system. However, significant modifications including the need for optical access, high costs, and setup complexity with limited robustness confine such measurement techniques to purpose-built test facilities. Thin-wire thermal sensors such as resistance wire thermometers (RWTs) and exposed thin-wire thermocouples best satisfy the measurement technique requirements with the benefit of easy integration to test rigs while remaining scalable within and across test setups.

As thin-wire welding limits the smallest thermocouple junction size [9], wire diameters below 12.7 µm have been pursued with RWTs. Benson [10] focused on the design and development of RWTs for EGT pulse measurements with 10 mm long tungsten wires between 6.9 µm and 25.4 µm. The wires were placed taut (supported and pretensioned) and used nickel sleeves over the weld faces for weldability. Benson [10] also indicated good robustness for 6.9 µm wires when engine speeds were below 1000 rpm. However, Caton [11] estimated only ~5 min of engine operation for RWTs below a diameter of 10 µm. RWTs are also susceptible to significant drift of the static calibration function by up to 50% from the baseline [4], owing to oxidation in the exhaust environment, which limits their test duration. Furthermore, dynamic error correction through dynamic calibration [4] or multiwire-based response compensation [10] remains necessary due to the small yet finite thermal inertia.

Multiwire-based response compensation (signal reconstruction) was predominantly pursued using Type-K thin-wire thermocouples. Mollenhauer [3] tested multiple two- and three-wire thermocouple sensors with wires over 5 mm long and diameters between 40 µm and 120 µm. A high-temperature cement was applied at each end of the taut thermocouple wires and indicated a maximum operational time of ~20 h. Kee et al. [12] utilized Tagawa et al.'s [13] reconstruction technique to estimate EGT transients (over seconds). Thermocouple wires of diameters 500 µm and 800 µm ($\leq$1.5–2× diameter ratio [13]) reconstructed a response similar to a 125 µm wire. In contrast to previous thin-wire-based studies in the engine context, the wires were slack (unsupported and without pretension). This construction is mechanically weaker compared to taut wires [14, 15] with Kee et al. [12] and Caton [11], indicating robust slack wire diameters of 125 µm and 254 µm, respectively, within their tests. However, subsequent studies [16, 17, 18, 19, 20] over the last 25 years utilizing thin-wire on-engine thermocouples for EGT measurements have predominantly adopted the slack wire design with significantly thinner wires.

Multiwire thermocouple studies by Kee et al. [16] and Kar et al. [17] developed reconstruction algorithms for the EGT pulse using slack wires with diameters of 12.5–50 µm and 50–125 µm. The reconstructed signal in these studies [16, 17], while successful in controlled environment tests, could not be established on-engine and did not have a reference EGT measurement. Morey et al. [19] (using a slack 25.4 µm wire measured EGT) and Kar et al. [18] (using the reconstructed EGT) established that the peak and mean EGT correlates with the cycle-to-cycle variations of the combustion process represented by the net and gross indicated mean effective pressure (IMEP), respectively. On the contrary, studies by Gardiner et al. [21, 22] utilized the EGT signal derivative of robust stepped sheathed thermocouples [23] to detect misfires and cycle-to-cycle variations without relying on the absolute instantaneous EGT value. Papaioannou et al. [20] extended the sensor design by Kar et al. [17] and highlighted that the measured mean EGT was observed to increase with the wire diameter. The greatest difference (40–80 K) was observed between the thin-wire thermocouples and the mineral insulated metal sheathed (MIMS) thermocouple. This was attributed to the combined effects of lower thermal inertia and an

increased significance of conduction heat transfer in smaller diameter wires [17].

The tested engine operating points in the aforementioned studies were typically in the low load range of 2–6 bar brake mean effective pressure (BMEP)/IMEP. The sensor was located downstream of a single-cylinder engine exhaust [16, 20] or located at or close to the exhaust port of a serial engine [17, 19]. Only Morey et al. [19] reported slack wire failure at the highest tested load point of 5.49 bar BMEP and recommend changing the measurement location to improve sensor robustness. However, the measurement location can be pertinent, for instance, at the exhaust port, where Caton and Heywood [4] reported a ±5–8% temperature variation when depth profiling the port exit.

Thus the limitations of existing thin-wire thermocouple studies in the ICE context for EGT measurements indicate the need for a robust sensor design. This includes determining the robustness limits of slack wire designs adopted in the reported literature over a range of engine operating points and measurement locations. Recent studies [24, 25] indicate that taut wires (5–12.5 µm) with coated weld faces using a silver-based paste [24] and a ceramic adhesive [25] improved the thin-wire sensor robustness. Operational times of over 80 h in a high-temperature flow rig (644 K and 455 m/s) [24] and around 1.5 h (from 7 min without a coating) at low ICE loads [25] were observed. The coated weld face is similar to Mollenhauer's [3] sensor design and could support the good robustness observed by Benson et al. [10] due to the nickel sleeves over the welds. Unlike RWTs, thin-wire thermocouple studies have predominantly overlooked static calibration and drift quantification, which could be a constraint for the test time. Furthermore, the efficacy of multiwire reconstruction techniques remains to be established on-engine. Papaioannou et al. [20] indicated that the measured thermocouple signals (inputs for the reconstruction techniques) need to be assessed for response sensitivities related to sensor design parameters.

This study evaluates the implications of thin-wire thermocouple sensor design in multiwire configurations on sensor robustness and response in the exhaust of a serial heavy-duty diesel engine. The assessed sensor design parameters included wire diameters between 51 µm and 254 µm and the wires mounted either slack or taut with coated weld faces. The exposed wire length was varied based on the protrusion length and ceramic bore spacing. Sensor robustness was assessed based on the time to wire failure, occurrences of wire deformation, and drift in the static calibration function. The sensor response was evaluated using the cycle-averaged temperature signal and its mean value. Unlike previous studies, the developed sensors were exposed to wide-ranging exhaust gas pulsating flow conditions by varying the measurement location and the engine operating point. The study elucidates the robustness limitations of commonly adopted slack wire designs in contrast to the coated weld face taut wire design. Furthermore, it motivates the need for utilizing and understanding improved accuracy cycle-resolved and mean EGT measurements from reduced-diameter thin-wire thermocouples with longer exposed lengths.

Sensor Design and Fabrication

This section briefly explains the relationship between thin-wire thermal sensor design parameters and their robustness and response. Subsequently, the sensor fabrication procedure adopted in this study is described.

Thin-Wire Thermal Sensor Design Theory

The thin-wire thermal sensor design is primarily defined by the wire diameter, the exposed wire length, and the thermophysical material properties of the wire. The wire length and diameter determine the length-to-diameter ratio (l/d), which is an important design parameter. Additionally, the sensing wire may be installed in the conventional taut design or the slack design. From the robustness perspective for a given material, a larger wire diameter and a shorter exposed length (lower l/d) reduces the stress induced in the wire by aerodynamic drag forces [14]. The exposed length (and l/d) may be kept low by minimizing the slack wire junction protrusion length and the spacing of wire leads between the ceramic bores. Furthermore, when the wire is mounted taut, the greater rigidity makes it resistant to flow-induced vibrations [14] unlike slack wires that have limited resistance to lateral loads [15].

From the response perspective governed by the heat balance of the sensor, a lower wire diameter with lower thermal inertia increases the frequency response for a given flow condition [9]. It also minimizes the impact of conductive and radiative heat losses due to a reduction in the cross-sectional and surface area of the wire [26]. A longer exposed wire improves convective heat transfer between the gas and the wire while minimizing the conductive heat transfer with the support wires. Contrary to the robustness requirement, this is achieved by increasing the junction protrusion length (slack wires) and the bore spacing (slack and taut wires). An l/d > 200 is considered sufficient to neglect conduction heat losses at a flow Reynolds number (~0.01) [26]. Mounting the wires slack or taut could affect the nature of convective heat transfer over the wire, although empirical formulations are developed for flow normal to taut cylindrical wires [27].

Thin-Wire Thermocouple Fabrication

Despite literature indicating a fabrication procedure for multiwire thermocouple sensors, the major challenge was to devise a fabrication process that limits the exposed thin wire as the weakest section of the entire sensor. Figure 1 illustrates the sensor fabrication process adopted in this study and presents the steps from the base materials used (1a) to the final fabricated sensor (1e).

FIGURE 1 Thin-wire thermocouple sensor (slack design) fabrication steps with (a) base materials, (b) pre-weld sensor assembly, (c) spot welding one leg of the thin wire, (d) ceramic-coated spot weld, and (e) complete sensor with slack sensing elements in the inset.

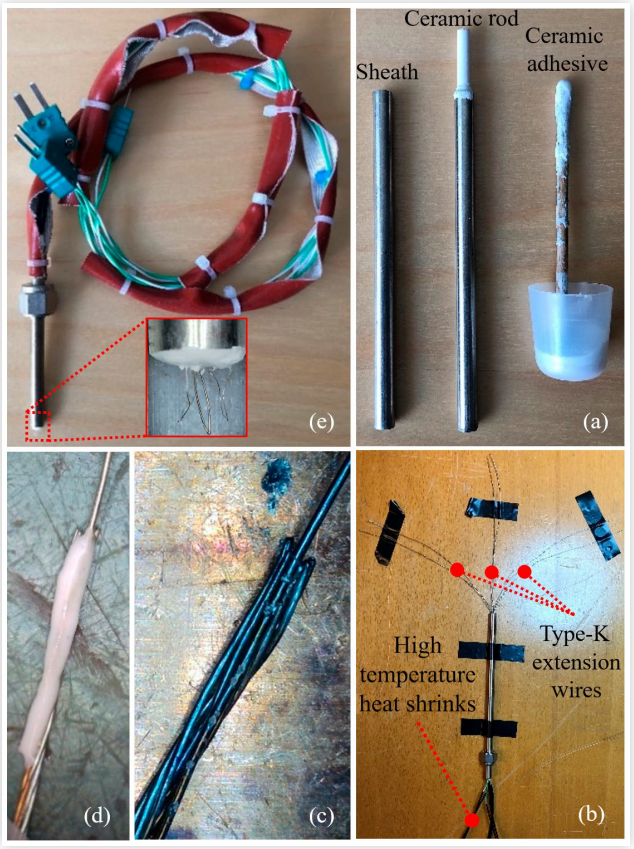

The base materials in Figure 1(a) include a metal sheath of 6 mm outer diameter (stainless steel) enclosing a 6-bore ceramic rod (Haldenwanger Pythagoras) with a 4.5 mm outer diameter. The 1.1 mm diameter boreholes of the ceramic rod houses and insulates the different thermocouple lead wires. A high-temperature ceramic adhesive (Cotronics Resbond® 940HT) bonds the ceramic rod within the sheath over a curing time of 24 h. The length of the sheath and rod can be varied as per requirement and was typically between 80 mm and 120 mm. Figure 1(b) highlights the use of stripped and stranded Type-K thermocouple extension wires (American Wire Gauge [AWG] 24) that are inserted from the rear end of the sensor body to twice the sensor body length with high-temperature heat shrinks. The thin-wire thermocouple legs are then welded to their matching polarity extensions. This approach of interfacing the thin-wire thermocouple to an extension wire was also adopted in a special aspirated probe design [16] in contrast to [17] and derived studies [20] wherein the thin-wire thermocouple leads were soldered onto connector pins. The purpose of welding onto a Type-K extension wire was to avoid the low melting temperature of solder over the prolonged operation. It also overcomes the uncertainty of introducing an intermediate junction at the connector interface. The adopted approach embeds the welded interface within the sensor body and avoids the risk of buckling at the connector end. The sensors were mounted onto male adapter fittings and required a corresponding cap-ferrule assembly to be swaged on the sensor body. The swaging location is adjusted to match the desired insertion depth. The cap and ferrule installation preceded welding the thin-wire thermocouples onto the extension wires.

The thin-wire thermocouple legs corresponded to over half the sensor body length and were spot welded onto the extension wires [Figure 1(c)] with ≥15 mm overhang. This was used to adjust the exposed thin-wire axial protrusion length. The weld face was ceramic coated [Figure 1(d)] to improve bond strength and avoid detachment when the extension wires were retracted from the rear end of the sensor. The wires were then retracted to achieve a comparable axial protrusion length of the thermocouple junction (~3–4 mm) to the literature [17, 20]. Junction spacing is strongly determined in one plane by the ceramic bore pitch (~1.3 mm in this study) and the wires had to be manually positioned closer to achieve spacing between ~0.5 mm and 1 mm. EGT signal reconstruction relies on the thermocouple junctions being closely spaced (≤0.5 mm) to maintain a high correlation and a low mean offset between the signals [16]. To fix the position of the thin wires in the ceramic borehole, a ceramic adhesive is applied during the wire pullback process and allowed to cure for 24 h.

Subsequently, the exposed extension wires at the rear end were insulated with the installed high-temperature heat shrinks and connected to independent screw on Type-K thermocouple connectors. Figure 1(e) depicts the final sensor assembly with a fluorinated ethylene propylene (FEP) insulated extension cable enclosed by a thermal insulation sleeve with 0.6–1 m length. The inset in Figure 1(e) shows the exposed thin-wire thermocouples left slack. The thin-wire thermocouples were procured pre-welded from Omega Engineering Inc. in bead and butt weld configurations. A Labfacility L60+ fine-wire welder was used to weld thin wires to the extension wires and also fabricate thermocouple junctions above 51 µm when required.

While Figure 1 details the typical fabrication process adopted in this study, taut design sensors differed in having thicker support wires (prongs) with 0.81 mm diameter. The prongs protruded ~3.5 mm from the sensor body as exposed extension wires at the sensing end. At the cable connector end, the prongs were either crimped with nickel splices or butt welded onto Type-K extension wires and embedded in the sensor body. Taut sensor designs are reusable as the failed thin wire at the sensing end may be replaced and the sensor body reused. In this study, a total of six independent multiwire thermocouple sensors were developed and tested. These included five sensors of the slack wire design derived from thermocouple studies [11, 12, 17, 19, 20] and one sensor of the taut wire design derived from RWT studies [3, 10, 24, 25]. Table 1 provides a summary of the geometric characteristics of sensors which includes the sensor label (name) and the wire

TABLE 1 Design specifications of the developed sensors.

Sensor label	Wire diameters [μm]	Design changes
Proto	51-127-76 butt weld	Baseline slack design target 4 mm axial protrusion
Slack-1	51-127-51	Baseline + ceramic-coated exposed wire base (upon testing)
Slack-2	51-127	Baseline + ceramic-coated exposed wire base
Slack-3	51-254-76 butt weld	Baseline + ceramic-coated exposed wire base and extension wire weld + lower axial protrusion 3 mm
Slack-5	127-51-254	Baseline + ceramic-coated exposed wire base and extension wire weld + lower axial protrusion 3.5 mm
Taut1-v1	51-76-76	Reusable 3.5 mm axial protrusion prongs + coated exposed weld faces (51-slack, 2× 76 taut)
Taut1-v2	76-76-76	Reusable 3.5 mm axial protrusion prongs + coated exposed weld faces (3× 76 taut)

diameter combination expressed in the format d_1-d_2-d_3, where d_2 indicates the wire located between d_1 and d_3. Table 1 also includes design feature changes related to the fabrication and protrusion or exposed wire lengths that affect the wire l/d.

Engine Experimental Setup

Engine experiments were performed on a Scania D13 inline six-cylinder heavy-duty diesel engine with a specially developed single-pipe exhaust. The specifications of the base engine are presented in Table 2. The primary change from the default engine configuration pertained to the exhaust layout. The runner of Cylinder-6 of the engine was replaced by a single-pipe exhaust with a dedicated flow measurement section that bypassed the turbocharger turbine stage. This setup implied that the variable geometry turbine (VGT) turbocharger was powered by five cylinders on the turbine side, while the compressor provided boost pressure for all six cylinders after passing through a water-cooled charge air cooler (CAC). The single-pipe exhaust merged with the main exhaust line of the remaining five cylinders after the EAT unit to a common passage leading to the test cell exhaust vent. The mean pressure at the exhaust vent was at the atmospheric level of ~1 bar absolute (refer to Figure A.1 in Appendix A). Figure 2 (top) provides a schematic representation of the engine setup and sensor measurement locations with the real setup depicted in Figure 2 (bottom). The exhaust manifold included two measurement locations shown in Figure 2 labeled Eman-1 toward Cylinder-1 and Eman-2 at the turbine inlet toward the Cylinder 1-2-3 bank. The Eman-1 location was used for an initial assessment of the sensor design, while Eman-2 was the primary test location in the exhaust manifold.

The single-pipe exhaust provided the possibility to isolate the exhaust pulse of a single exhaust event from the interactive effects of other cylinders. The single pipe had no backpressure to evoke the highest intensity exhaust pulses for a given operating condition. A flow development length (Figure 2) was provided to minimize spatial gradients in the exhaust gas velocity and associated bulk temperature field along the pipe

TABLE 2 Engine specifications.

Engine	Scania D13
Emission compliance	Euro VI
Configuration	Inline-6
Firing sequence	1-5-3-6-2-4
Displacement	12.7 liter
Bore	130 mm
Stroke	160 mm
Connecting rod length	255 mm
Nominal compression ratio	18:1
Turbocharger	Holset VGT
Exhaust valve open	125 CAD aTDCf
Exhaust valve close	373 CAD aTDCf
Warm engine coolant temperature	80 °C
Warm engine oil temperature	90–100 °C
Fuel	B0 diesel

FIGURE 2 Schematic of the engine experimental setup (top) and corresponding implementation in the test cell (bottom).

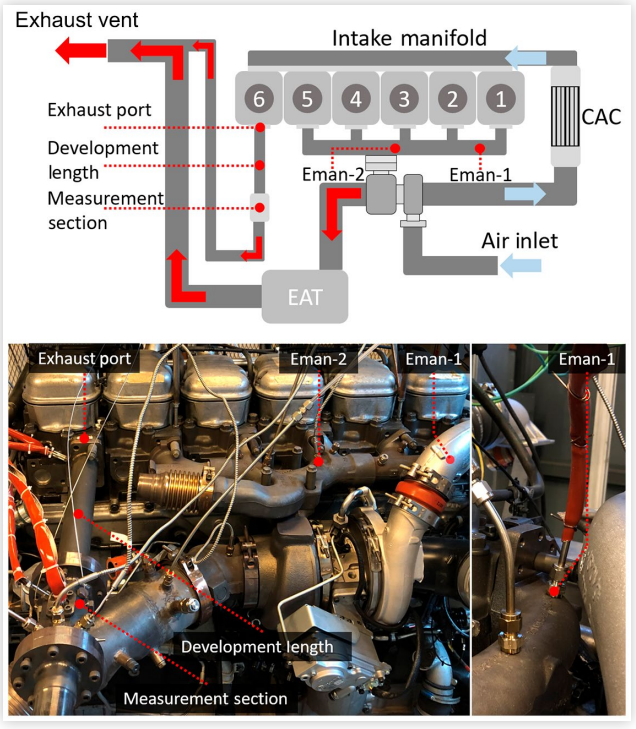

cross section at the measurement section. Additionally, invasive sensor testing can be performed in the single-pipe setup without the consequence of broken sensor parts entering the turbocharger turbine at the early stages of sensor development.

Flow development guidelines for turbulent flows in circular pipes with bends and contractions at the inlet typically indicate a hydrodynamic development length between 10 and 60 times the pipe diameter (L/D) [28, 29]. While these guidelines do not translate to the pulsatile flows in the exhaust of ICEs, practical setup limitations constrained the single-pipe L/D ~10 times the pipe diameter (40 mm). This led to a flow development length section of 400 mm preceding the measurement section. The measurement section includes mating flanges and some clearance that distances the measurement plane to an L/D of ~11. The single pipe and the measurement section were not thermally insulated or conditioned, owing to accessibility requirements.

An AVL DynoDur 500 dynamometer regulated the engine speed and load. Target test parameters were achieved through accessible control variables like the fuel injection timing and quantity, fuel rail pressure, and the VGT rack position of a partially open electronic control unit (ECU). Mean pressure and temperature levels were measured across various engine locations to monitor the engine boundary conditions. The measurement section included a 3 mm and 6 mm Type-K MIMS thermocouple to provide the reference EGT. Bolt-on washer wall thermocouples (Type-K) were mounted on either side of the measurement section to measure the outer wall temperature. An infrared gun provided real-time feedback on the wall temperature of the measurement section or the exhaust manifold to monitor thermal stability. Airflow to the engine intake was measured using an Annubar, while an AVL 733s fuel scale measured the total fuel flow. Table 3 lists the specifications of the slow logged sensors used to monitor mean levels of different parameters in this study.

TABLE 3 Engine slow logged sensor specifications.

Parameter	Sensor	Range	Specification
Gas pressure	GEMS 3500	±0.3 bar gauge 0–6 bar gauge	±0.25% FS (accuracy)
Gas temperature	Pentronic 3, 6 mm MIMS Type-K	–200 °C to 1200 °C	Greater of ±2.5 °C or ±0.75% of reading (IEC 60584)
Wall temperature	Pentronic bolt-on washer Type-K	<400 °C	Greater of ±2.5 °C or ±0.75% of reading (IEC 60584)
Wall temperature (infrared monitor)	Testo Quicktemp 860-T3	–30 °C to 900 °C	±0.75% of reading (accuracy 75–900 °C)
Fuel flow	AVL 733s	0–150 kg/h	0.12% (uncertainty)

TABLE 4 Engine crank angle–resolved (fast) sensor specifications.

Parameter	Sensor	Range	Accuracy
Cylinder pressure	Kistler 7061B (water cooled)	0–250 bar	≤ ±0.5% FS
Intake gas pressure	Keller M5HB	0–10 bar abs	±0.1% FS
Exhaust gas pressure	Keller M8coolHB (water cooled)	0–10 bar abs	±0.1% FS

Crank angle–resolved (fast) pressure measurements primarily focused on the intake, in-cylinder, and exhaust port pressures of Cylinder-6 beside the static pressure at the measurement section. Fast pressure measurements were also performed at the exhaust manifold when required. Table 4 summarizes the fast pressure sensor specifications. While the piezoresistive pressure sensors had an integrated amplifier unit, the cylinder pressure sensor utilized a Kistler type 5011 charge amplifier. The fast thermocouples utilized a custom-built six-channel amplifier module based on the AD597 (Type-K) and included cold junction compensation. The base scaling factor of the amplifier is 10 mV/°C for the range –20 °C to 350 °C [30]. A passive low-pass filter with a cutoff frequency of 10 kHz was applied to the amplified output signal comparable to the 13 kHz cutoff set by Kar et al. [17]. Sensor mounting was typically at an insertion depth of 15 mm at the measurement section (5 mm above the pipe centerline) and at the pipe centerline at the exhaust port and exhaust manifold, unless otherwise specified. Insertion depth uncertainty was estimated to be within ±2 mm at the exhaust port and within ±1 mm at the other locations. The wires were always aligned to match the corresponding pipe axis of the location.

Table 5 summarizes the specification of the instrumentation used for chain calibrating the pressure and temperature sensors. The fast intake and exhaust gas pressure sensors were calibrated by the manufacturer. The resulting calibration functions were implemented as correction parameters in the data acquisition (DAQ) software for the slow logged measurements, while the fast measurements were postprocessed with their respective calibration function. Crank angle–resolved measurements were sampled at 0.1 crank angle degree (CAD) resolution over 300 cycles using an 8-channel 12-bit PowerDAQ analog-to-digital converter (ADC) card. Simultaneous slow measurements were sampled at 1 Hz over 1 min using an in-house developed code. Unless otherwise specified, the slow logged and crank angle–resolved engine logs were performed on a warm engine (refer to Table 2 for coolant and oil temperature levels) upon attaining thermal equilibrium at each of the test points.

Experimental Method

This section begins by providing a theoretical basis and implementation of the engine experimental design. This is followed

TABLE 5 List of sensor calibrators.

Parameter	Calibrator	Range	Accuracy
Gas pressure (GEMS 3500)	Druck DPI 705 manometer	0–20 bar	±0.1% FS
Thermocouples MIMS/bare wire	Isotech Quick-Cal High Temperature	30–350 °C	±0.1 °C to ±0.4 °C
Cylinder pressure	Ametek HydraLite Tester	1–150 bar	±0.05% of reading
Wall thermocouples	VWR hotplate/stirrer	30–400 °C	±2% stability

by highlighting the exhaust conditions representing the temperature and pressure levels endured by the sensors over different engine operating points and measurement locations. Subsequently, details of the procedure adopted for static calibration of the measurement chain of thin-wire thermocouples and sensor drift tracking are discussed. The test sequence for the sensors listed in Table 1 concerning engine operating conditions and measurement locations ensues. The section concludes with the adopted approach for sensor response assessment and delineates the on-engine limitations.

Engine Experimental Design and Implementation

The engine test matrix (Figure 3) was determined from an exhaust valve discharge perspective that focused on isolating engine speed and load effects on the resulting exhaust pressure and temperature pulses in the single pipe. The objective was to provide an idealized on-engine flow environment at the measurement section for the tested sensors. Four load sweep points (LS1-4) increased the pulse intensity with the load (500–1000 Nm) for a given valve opening speed (at 1500 rpm). Additionally, four speed sweep points (SS1-4) with a comparable single-pipe exhaust mass flow (normalized by engine speed) primarily varied the valve opening speed with engine speed (700–1900 rpm). A common operating point (LS2 and SS3) ensured repeatability checks across the sweeps. To ensure comparable conditions across the test points, the single-pipe EGT and exhaust mass flow (details shared in Appendix A) were set as target variables. The single-pipe target EGT used the 3 mm MIMS thermocouple at the measurement section.

FIGURE 3 Engine operating points with labels (LS-load sweep and SS-speed sweep) including the net IMEP of Cylinder-6 (mean ± 2σ).

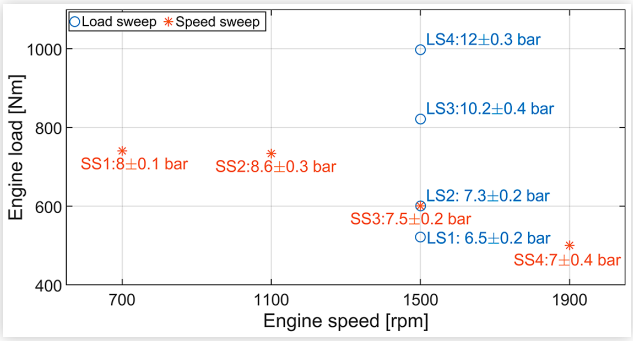

Figure 3 also includes the mean and two standard deviations (±2σ) of the net IMEP of Cylinder-6.

Tests commenced with a warm-up phase of the engine that typically lasted for 30 min at 1100 rpm and load steps between 200 Nm and 600 Nm. The rate of wall temperature change at the measurement section or exhaust manifold (depending on sensor location) was used as the criteria to repeatedly determine thermal equilibrium and was set at <1 °C/min. This corresponded to a minimum of 15 min of steady operation at each of the test points. In most cases, the sensors were mounted after the completion of the warm-up phase, unless otherwise specified. Sensor checks were performed for visual inspection with a handheld digital microscope and/or repeat static calibrations intermittently between test phases, for example, between the speed and load sweeps. Microscope images were calibrated for estimating junction spacing and the wire l/d with respect to the wire diameter even for bead-welded thin-wire thermocouples using ImageJ software. An image resizing plugin [31] was used for scaling the images.

Exhaust Conditions at Different Sensor Locations

As the focus of this study pertains to the conditions faced by the sensors, representative gas pressures and temperatures over the engine test matrix at different measurement locations are summarized. Figure 4 highlights the expected mean gas

FIGURE 4 Static pressure at different measurement locations and engine operating points. The whiskers denote the maximum and minimum instantaneous pressure levels experienced at these points while the marker "*" indicates the mean pressure.

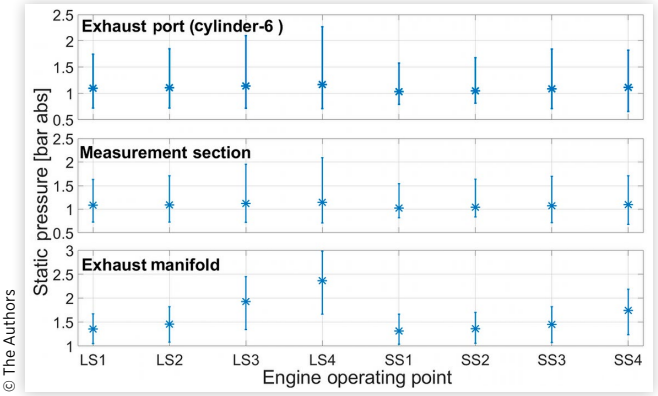

FIGURE 5 Mean temperature levels at different measurement locations and engine operating points where whiskers denote the ±2σ standard deviation experienced at these points.

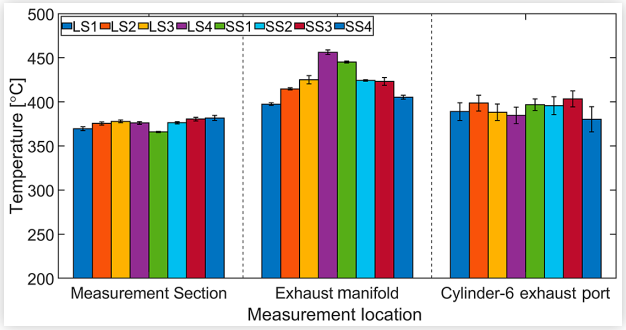

FIGURE 6 Temperature deviation observed between the calibrator reference temperature and thermocouple output amplified at base scaling (10 mV/°C) over the calibrated temperature range.

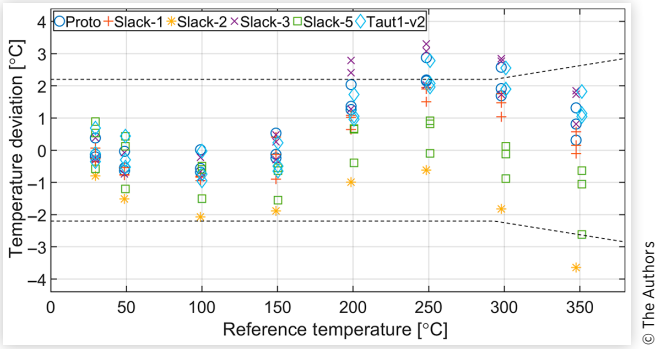

pressure using the fast pressure sensors. Figure 5 showcases the mean EGT using the 3 mm MIMS thermocouples. The data used in these figures are from experiments performed with the Slack-1 sensor. As the exhaust port did not have a reference MIMS thermocouple, the mean value of the Slack-1 127 µm wire is used as a representative measure in Figure 5.

Figure 4 indicates a mean static pressure at the exhaust port and measurement section ~1 bar abs. Higher mean pressure levels are noticeable at the exhaust manifold due to backpressure from the VGT and the EAT. The whiskers in Figure 4 indicate the maximum and minimum pressure levels at the different locations and highlight the unsteadiness and pulse intensity experienced by the sensors. In Figure 5, the EGT levels at the measurement section appear comparable by experimental design at ~375 ± 11 °C. The EGT observed at the other measurement locations is representative of the engine settings used to achieve the target metrics at the single pipe. In Figure 5, the higher mean EGT variation at the exhaust port (over 300 cycles) is due to the thinner 127 µm bare-wire thermocouple in contrast to the 3 mm MIMS (sampled over 1 min steady operation) at the other measurement locations.

Thin-Wire Thermocouple Calibration and Drift

Static calibration of the thin-wire thermocouple measurement chain was performed in a dry-well calibrator oven between 50 °C and 350 °C at 50 °C intervals. The calibration protocol involved preheating the calibrator to 30 °C as a common starting point. A typical soak time at each temperature level was 15 min, followed by data logs over 2 min at a sampling rate of 10 kHz. Figure A.2 and Table A.2 (see Appendix A) detail the pre-test linearity of all wires and the chain calibration functions for data analyzed in the study. All thin-wire thermocouple signals utilize the listed calibration functions with extrapolation where the measurement exceeds the calibrated temperature range. Drift tracking involved repeating the static calibration procedure through test intervals or after completion of the engine test matrix with different sensors. The number of post-test calibrations and the intermittent duration varied across sensors, depending on the test sequence and robustness of the sensor.

To highlight the significance of thermocouple tolerance, Figure 6 depicts the temperature deviation when using the base scaling of the amplifier (10 mV/°C) to the reference temperature of the calibration oven. The dashed lines indicate Class-2 thermocouple tolerance levels (ASTM E230/E230M-12: ≥ ±2.2 °C or ±0.75%).

Figure 6 shows a widening spread across the sensors and even between multiple wires of the same sensor as the reference temperature increases. The deviation induced by the entire measurement chain for all wires/sensors before experiments fall within the thermocouple tolerance band except between 200 °C and 300 °C. The thermocouple measurement chain accuracy can be significantly reduced to ≤ ±0.4 °C with static calibration using this calibrator. Calibration holds increased significance when considering applications like signal reconstruction that are sensitive to offsets [16, 17] and utilize the measured signals and their time derivatives to estimate the true EGT. The skew in the reference temperature among the data points (x-axis) in Figure A.2 and Figure 6 is due to differences in the insertion depth of the various sensors in the calibration oven.

Thin-Wire Thermocouple Sensor Test Sequence

Table 6 summarizes the sensor test sequence indicated with Roman numerals while specifying the tested measurement location and the engine operating points. Detailed test summaries of the individual sensors are provided for all the sensors in the Appendix under Tables A.3 and A.4. Repeated instances of Roman numerals indicate a simultaneous test. Table 6 shows that sensor tests commenced with the slack design at the measurement section followed by tests at the other locations with different wire diameter combinations.

TABLE 6 Sensor test sequence.

	Measurement section	Exhaust port	Exhaust manifold
Proto	I: LS2	III: Warm-up + SS1-4 + LS3-4 (upper)	Not tested
Slack-1	II: LS1-4, III: SS1-4 + LS3-4	VIII: LS1-4 + SS1-4 (centerline)	IV: LS1 (Eman-1)
Slack-3	V: LS1-4 + SS1-4	Not tested	VI: LS1-2 (Eman-2)
Taut1-v1	Not tested	VII: SS1-2,4 + LS3-4 (centerline)	Not tested
Taut1-v2	Not tested	Not tested	VIII: Warm-up + LS1-4 + SS1-4 (Eman-2)
Slack-2	Not tested	Not tested	IX: Warm-up + SS1 (Eman-2)
Slack-5	X: SS1-3 + LS3-4	XI: SS1-4 (centerline)	Not tested

Subsequently, taut design sensor tests focused on the exhaust port and manifold locations, while slack design sensors were tested for repeatability.

Sensor Response Assessment and Limitations

The response of thin-wire thermocouples is assessed using both the cycle averaged (ensemble averaged) and the mean value (time average) of 300 complete engine cycles. The cycle-averaged signals are processed using a polynomial smoothening filter (2nd-order Savitzky-Golay filter [32]) with a sample length of 10 CAD, i.e., 101 samples. This filter type is prevalent in temperature signal reconstruction studies [13, 17] for computing signal derivatives. The ±2σ spread of the mean temperature is used to indicate the wire response sensitivity to cycle-to-cycle variations.

On-engine sensor response assessments have several limitations owing to both the nature of the measurement technique and the complexity of the engine exhaust environment. When comparing invasive sensors, it is physically impossible for them to measure at the same location making the measurements distinct in space. This applies even to multiwire sensors in this study as the junction spacing achieved was between ~0.5 mm and 1 mm for the slack sensors and ~1.3 mm for the taut sensors. Factors such as nonhomogeneity in the flow and temperature fields, variations in bead diameter for a given wire diameter, support wire boundary layer–induced attenuation for the taut sensors, and the instantaneous heat balance of the sensor also influence the sensor response. Therefore, thin-wire sensor response sensitivities may be clearly assessed only when the design parameter changes are of greater significance than the abovementioned interactive effects.

Results and Discussion

This section begins by providing an overview of the observed sensor robustness of all sensors tested through their exposure to respective engine operating points and measurement locations. The overview includes computing drift in the static calibration function. Subsequently, the slack and taut sensor designs are assessed at the different measurement locations for the nature of observed wire failure and/or deformation. The corresponding tradeoff in sensor response is highlighted with variations in wire diameter and exposed wire length (l/d) for a subset of the experiments performed.

Observed Sensor Robustness and Drift

A condensed quantitative graphical summary of the operational time of all thin-wire thermocouple sensors based on Tables A.3 and A.4 in Appendix A is illustrated in Figure 7. The figure characterizes the sensors based on the thermocouple wire diameters and their cumulative operational time on the engine. The wires are color coded according to their respective sensor labels while hatched patterns denote the measurement locations. Markers indicate the observation of wire mechanical deformation (▼) and failure of the wire (×).

Figure 7 indicates a bias toward testing thinner wires (51 µm and 76 µm) as the motivation was primarily to obtain the highest frequency response while determining the on-engine robustness. Figure 7 shows an increasing cumulative operational time with wire diameter wherein the thicker slack wires (127 µm and 254 µm) were typically limited by the test time of the thinner wire pairs and did not deform or fail through engine operation. All 51 µm and 76 µm slack wires were tested to failure across all measurement locations. Only one 127 µm

FIGURE 7 Operational summary of all sensors characterized by wire diameter, time at each measurement location, and cumulative operational time (total test time).

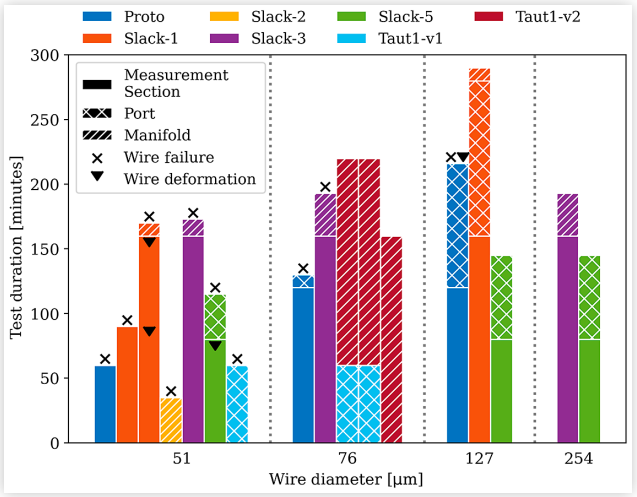

slack wire (Proto sensor) deformed and failed when tested at the exhaust port and located above the pipe centerline. Additional wire deformations were noticeable only for the Slack-1 and Slack-5 51 µm wires. It is noteworthy that the test points before visual inspection for all the 51 µm wire deformation cases were the highest load points LS4 (refer to II, III, and X in Table 6). LS4 had the highest peak-peak pressure variation as seen in Figure 4 (measurement section and port).

Figure 7 also showcases the limited operational time of 51 µm and 76 µm slack wires at the exhaust port and manifold. This was typically well within an hour of operation while better enduring conditions at the measurement section (over 2.5 h). Some bias was inherent in the test method that prioritized measurement section tests before the exhaust manifold (refer to Slack-1 and Slack-3 at the exhaust manifold in Table 6). However, the Slack-2 sensor was tested at the exhaust manifold with preloading only from the static calibration process which showed a limited increase in 51 µm slack wire operational time to ~0.5 h. Taut wires (Taut1-v1 and Taut1-v2) with thinner 76 µm wires indicated operational times comparable to thicker (127 µm and 254 µm) slack wires within 3.5 h and endured the entire test matrix without wire deformation or failure.

The observations in Figure 7 show that the robustness limitations of thinner slack wires (below 76 µm) and the greater robustness of thicker slack wires (127 µm and 254 µm) are in agreement with both sensor design theory (refer to thin-wire thermal sensor design theory) and the literature [11, 12]. It also shows that the ceramic-coated weld faces applied to Taut1 (v1 and v2) protect the welds and enhance sensor operational time in harsh conditions. The three 76 µm wires of Taut1-v2 endured the entire test matrix from the warm-up phase at the exhaust manifold. This supports observations in the literature [3, 10, 24, 25] and reaffirms that protecting the stress-concentrated weld faces of thin wires with a (ceramic) coating improves thin-wire sensor robustness.

Apart from considering sensor robustness from a purely structural perspective, drift in the thin-wire thermocouple static calibration trace was analyzed to determine its significance under ICE exhaust conditions. Figure 8 consolidates the computed drift of all tested sensors lumped at the sensor level between their first (Figure A.2 and Table A.2 in Appendix A) and final (post-test) static calibrations. The duration over which the sensor drift was computed is listed beside the sensor labels in Figure 8.

It is visible in Figure 8 that the drift in the static calibration trace in the 30–350 °C range is within the calibrator oven accuracy range (refer to Table 5) and hence can be considered insignificant in this study. This is a promising indication for utilizing thin-wire thermocouples over longer test durations with minimized periodic static calibrations. However, generalizing the robustness of such sensors from the perspective of thin-wire thermocouple drift requires further tests with prolonged test times at higher exposed and calibration temperatures.

Sensor Design Assessment at the Measurement Section

Figure 9 illustrates limitations in Slack-1, Slack-3, and Slack-5 sensors by comparing each of the sensors before and after tests in the measurement section. The Slack-1 (LS and SS) in Figure 9 indicates wire failure and deformation (along the pipe axis) of the 51 µm wires with 4 mm protrusion over the load sweep (2.8 mm deformation of 51a) and the speed sweep test points (1.5 mm deformation of 51a). The deformation occurred despite ceramic coating the base and repositioning the junction of the surviving 51a wire before the speed sweep test. However, the Slack-3 sensor in Figure 9 with a lower protrusion length (3 mm) showed no noticeable wire deformation. The reduction in junction protrusion by 1 mm reduced the 51 µm wire l/d of Slack-1 51a (160) and Slack-1 51b (175) to 115 for the Slack-3 51 wire.

Similarly, the Slack-5 sensor in Figure 9 with an intermediate protrusion of 3.5 mm indicated a 0.6 mm wire deformation of the 51 µm wire. This is attributed to the greater spacing between the wire leads when located in the middle of the ceramic rod which resulted in a l/d of 140. The deformation and failure observations of these 51 µm wires in Figures 7 and

FIGURE 8 Drift summary of all sensors computed between first and final static calibrations. The accuracy range of the calibrator oven is indicated by the dashed lines (±0.1 °C) and the figure bounds (±0.4 °C).

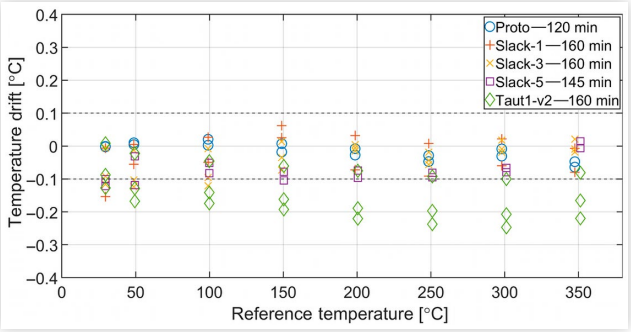

FIGURE 9 Wire deformation and failures of slack sensors observed at the measurement section.

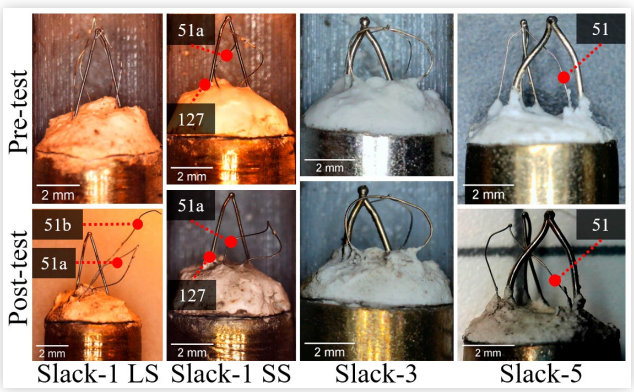

9 indicate a greater propensity to wire deformation with an increasing l/d from 115 to 140–160 which is supported by the literature (refer to thin-wire thermal sensor design theory). Taut wire sensors were not tested at the measurement section as the subsequent slack design sensors (Slack-3 and Slack-5) indicated sufficient robustness.

The wire l/d-related deformation is undesired during operation as it introduces a thermocouple junction location uncertainty in the measurement. This could also be detrimental to EGT signal reconstruction techniques. The implications of the wire length (l/d) on sensor response were pursued for the Slack-1 51a and 51b wires over the LS test points as shown in Figure 10. The mean value differences (legend of Figure 10) over LS1-4 between the 51a and 51b wires were consistent at 2 °C. The mean of 51a was higher despite its lower l/d of 160 indicating the significance of other factors (exhaust flow). The difference in cycle-to-cycle variations in the mean temperature (±2σ spread) was within ±1 °C with 51a showing a lower sensitivity. The cycle-resolved traces show that the peak-peak differences in measured temperatures between the 51a and 51b wires increased from 12 °C to 20 °C across LS1-4. The greater sensitivity of 51b can be attributed to its higher l/d which minimizes the impact of conduction heat loss (refer to thin-wire thermal sensor design theory).

While l/d changes of the 51 µm slack wires of the Slack-1, Slack-3, and Slack-5 sensors appear to have a significant impact on the structural properties (deformation) of the sensor, the implications on response seem insignificant when considering the measured mean and cycle-to-cycle variations of Slack-1 51 µm wires. However, the measured peak-peak temperature changed significantly when the l/d increased from 160 to 175, indicating a greater significance of exposed wire length on cycle-resolved EGT measurements.

While Figure 9 elucidates the robustness limitations of the thinner slack wires (51 µm), the implication of an increase in wire diameter on the sensor response is evaluated with all wires of the Slack-3 sensor and the Slack-1 127. Wire responses are compared over two engine operating points which depicted the maximum (LS4) and minimum (SS1) variation in mean temperatures among the thin-wire thermocouples. Figure 11 illustrates the cycle average and mean temperatures of the different wires at LS4 along with the reference 3 mm MIMS measured with Slack-3. The cycle-resolved traces present the gains in frequency response with a decreasing wire diameter (refer to thin-wire thermal sensor design theory). While the 254 µm wire only measures a peak-peak fluctuation of 12 °C, the 51 µm wire measures 80 °C and better captures the EGT waveform.

When considering the mean temperatures in Figure 11, it increased by 14 °C when increasing the wire diameter from 51 µm to 254 µm. The trend of an increasing mean temperature with an increase in wire diameter is consistent with observations by Papaioannou et al. [20] (on-engine) and Chomiak et al. [6] (analytical). The Slack-1 127, however, measured the same mean as the Slack-3 254. The convergence between the two mean temperatures despite doubling the wire diameter could be attributed to two factors. First, the mean reference temperature level for Slack-1 was 4 °C higher than the Slack-3 3 mm MIMS. Additionally, the greater exposed length of Slack-1 127 deduced by the increased scaling of l/d by a factor of three (20 to 60) explains the reduced significance of heat conduction for the thermocouple junction of Slack-1 127 over Slack-3 254.

It is also clear from Figure 11 that the sensitivity to cycle-to-cycle mean temperature variations decreased with an increase in wire diameter. The ±2σ spread of the measured mean temperatures decreased from ±10 °C (51 µm wire) to ±4 °C (254 µm wire). Interestingly, this aspect has not been explicitly highlighted or quantified in literature even when focusing on cycle-to-cycle temperature variations as they make use of EGT reconstruction [18] or a single thin wire for such estimates [19]. However, these studies [18, 19] acknowledge that increasing the wire diameter and its thermal inertia reduces the sensor sensitivity and signal-to-noise ratio. Thus, the sensor response benefits when lowering the wire diameter (at LS4) include a greater measured peak-peak temperature, an increased sensitivity to cycle-to-cycle mean temperature variations along with a better indication of the mean EGT. These observations demonstrate the need for lowering the wire diameter of thin-wire thermocouples for more accurate EGT measurements.

FIGURE 10 Mean ± 2σ and 300 cycle-averaged temperatures of the Slack-1 51a and Slack-1 51b wires over LS1-4.

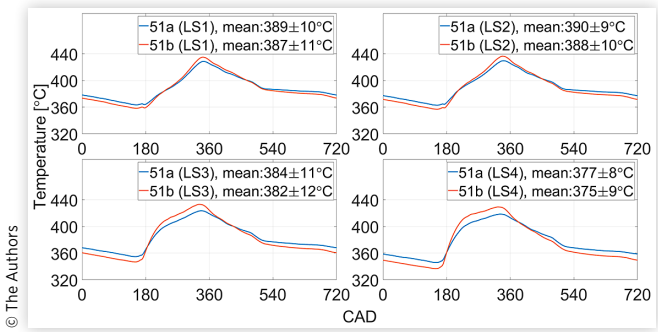

FIGURE 11 Mean ± 2σ and 300 cycle-averaged temperatures of the Slack-3 and Slack-1 127 at LS4.

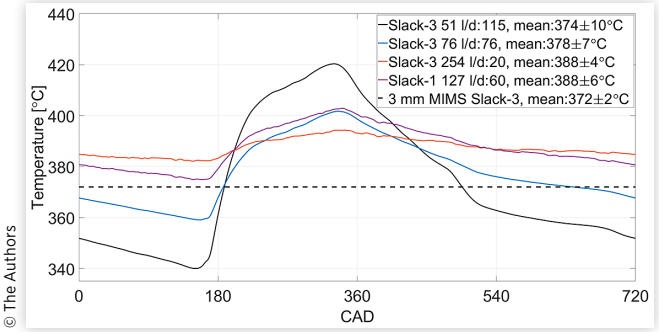

FIGURE 12 Mean ± 2σ and 300 cycle-averaged temperatures of the Slack-3 and Slack-1 127 at SS1.

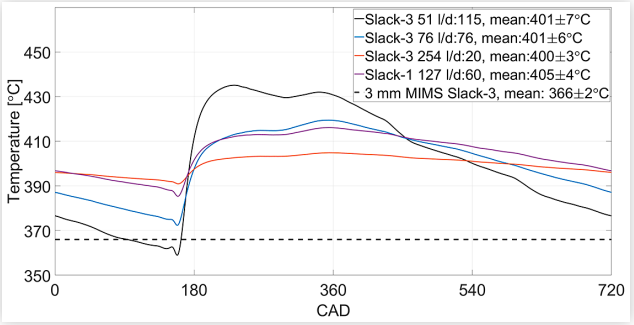

FIGURE 13 Proto 76 µm and 127 µm wires pre/post exhaust port test (upper).

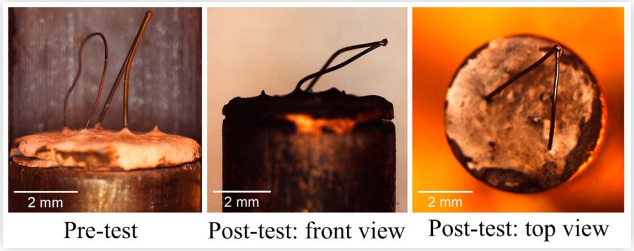

FIGURE 14 Slack-1 and Slack-5 sensors pre/post exhaust port test (centerline).

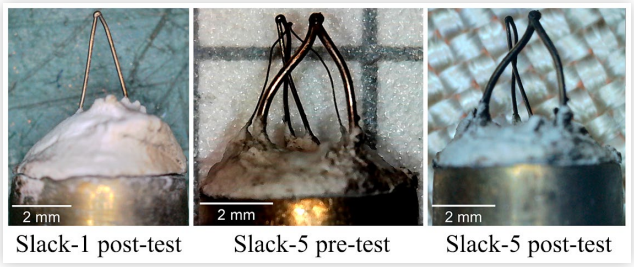

Figure 12, however, shows the sensor response sensitivities at the minimum mean temperature variation point (SS1). Similar to observations in Figure 11 at LS4, a reduction in wire diameter increased the measured peak-peak temperature from 14 °C (254 µm) to 76 °C (51 µm). Similarities to LS4 were also retained in the wire diameter sensitivity to the cycle-to-cycle mean temperature variation which reduced from ±7 °C (51 µm wire) to ±4 °C (254 µm wire). However, mean temperature differences were within 1 °C for the Slack-3 wires (51 to 254 µm). The 5 °C higher mean of Slack-1 127 could be attributed to a higher reference mean temperature from the 3 mm MIMS thermocouple (by 1 °C) and the l/d scaling as discussed in the LS4 case.

The insignificance in mean temperature variation at SS1 highlights the influence of the exhaust flow condition on the heat balance of sensors which requires further investigation. It also limits the possibility to generalize mean measured EGT trends with the wire diameter of thin-wire thermocouples in ICEs. However, the observations in Figure 12 show that the benefits of measuring greater peak-peak temperatures and cycle-to-cycle mean temperature variations are retained when lowering the wire diameter.

Sensor Design Assessment at the Exhaust Port

Slack Sensors at the Exhaust Port (Upper and Centerline) The exhaust port is expected to have a highly nonhomogeneous flow and temperature field with the flow concentrated toward the upper regions of the pipe at the port exit due to bulk inertia effects. Figure 13 illustrates the limitation of slack wires when placed 5 mm above the centerline at the port exit with significant wire deformation and failure of even the Proto sensor 127 µm wire. Unlike wire failures at the measurement section, the Proto sensor 127 µm wire was mechanically intact (Figure 13) and presumably failed due to severe oxidation after 1.5 h of operation at the port.

With an anticipated reduction in pulse intensity at the exhaust port centerline, Figure 14 shows the feasibility of slack wire tests at this location through the Slack-1 (only 127 µm wire) and Slack-5 sensors (all wires). While the larger 127 µm and 254 µm slack wires endured their respective test cycles without noticeable wire deformation, the pre-tested Slack-5 51 (refer to X and X1 in Table 6) failed after 35 min of operation at SS2. Observations in Figures 13 and 14 thus highlight the conditional operability of slack wires at the exhaust port pertaining to both wire diameter and protrusion depth in the pipe.

Taut Sensors at the Exhaust Port (Centerline) Figure 15 illustrates the Taut1-v1 sensor before and after tests at the exhaust port centerline. It is observable that the taut wires (76a and 76b) endured the test conditions and retained their junction positions until the 51 µm slack wire failed at SS4 after 1 h (refer to VIII in Table 6). Although physically robust at the exhaust port, the taut wires in Taut1-v1 have a lower exposed wire length and l/d of 34 (76a) and 12 (76b). The slack 51 µm wire had an l/d estimated over 50. The considerably lower l/d of Taut1-v1 wires compared to Slack-3 51 and Slack-3 76 wires (Figure 12) favors sensor robustness over response (refer to the thin-wire thermal sensor design theory).

The Taut1-v1 sensor response tradeoff related to the wire diameter and l/d is highlighted in Figure 16 by comparing the cycle-averaged temperature signal and mean temperatures of the wires at SS1. Similar to observations with Slack-3 at the measurement section (Figures 11 and 12), the cycle-averaged temperature signals in Figure 16 show a significantly higher frequency response when decreasing the wire diameter from 76 µm to 51 µm. It is also evident in Figure 16 that a reduction in the l/d (exposed wire length) from 34 to 12 attenuates the response of the 76b wire similar to observations with Slack-1 51a at the measurement section (Figure 10). The peak-peak

FIGURE 15 Taut1-v1 sensor pre/post exhaust port tests at the pipe centerline.

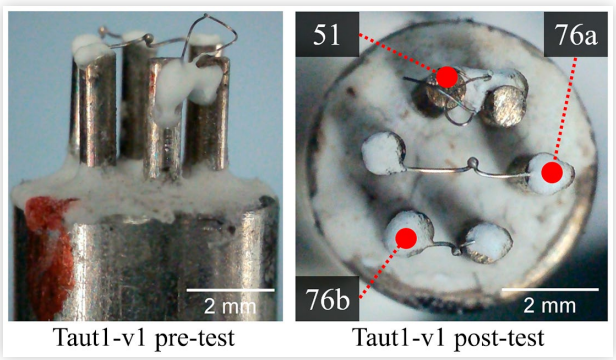

measured temperature decreased from 173 °C for the 51 µm wire to 81 °C (76a) and 56 °C (76b) for the 76 µm wires.

The mean temperatures for the Taut1-v1 wires in Figure 16 showed dependencies related to both the wire diameter and wire l/d. The 51 µm wire measured a mean that was 26 °C lower than the 76a wire while the lower l/d 76b wire recorded a mean that was 17 °C lower than 76a. The mean temperature reduction when lowering the wire diameter was established with the Slack-3 sensor at LS4 in the measurement section (Figure 11). However, the expected reduction in mean temperature with an l/d reduction due to a greater significance of conduction heat loss (refer to the section Thin-Wire Thermal Sensor Design Theory) is now visible in the lower mean indicated by the 76b wire in Figure 16. This is contrary to the l/d insensitivity and inverted trend to the mean temperature of the Slack-1 51 wires at the measurement section (Figure 10).

When considering the cycle-to-cycle variations of the mean temperatures (±2σ) in Figure 16, it decreased with an increase in wire diameter from ±12 °C (51) to ±6 °C (76a). It also decreased when reducing the wire l/d from ±6 °C (76a) to ±4 °C (76b). These observations indicate the detrimental impact of increased thermal inertia (with wire diameter) and a higher conduction heat loss (with lower l/d) on the mean and cycle-resolved measured temperatures of thin-wire thermocouples (refer to the section Thin-Wire Thermal Sensor Design Theory). Therefore, the observations in Figure 16 indicate that smaller diameter wires and longer exposed lengths for a given wire diameter (higher l/d) are required for more accurate EGT measurements.

Sensor Design Assessment at the Exhaust Manifold

Figure 17 shows the failure of different slack wire sensors along with the robust taut wire sensor (Taut1-v2) when tested at the exhaust manifold. The limited resistance of the slack design to lateral loads (refer to the section Thin-Wire Thermal Sensor Design Theory) and the inherent nonhomogenous flow field in the exhaust manifold could explain their limited operational time at this measurement location. Additionally, the wires face increased loading from multiple pulses per cycle at a higher reference mean EGT and pressure level at the exhaust manifold (refer to exhaust manifold in Figures 4 and 5) compared to the other measurement locations.

The robust Taut1-v2 sensor comprised 76 µm wires with different l/d (exposed wire lengths) between 8 (76n in Figure 17) and 34. Similar to observations at the exhaust port (Figure 16), the reduction in wire l/d was expected to detrimentally impact both the mean and cycle-resolved temperature measurements. This could be attributed to an increase in conduction heat loss with a lower exposed wire length (refer to the section Thin-Wire Thermal Sensor Design Theory). Figure 18 illustrates the cycle-averaged signals and mean temperatures at SS1 of the Taut1-v2 sensor located at Eman-2 in the exhaust manifold.

The cycle-averaged temperature signals in Figure 18 appear comparable over the engine cycle contrary to the clear differences in the cycle-resolved temperatures between the 76a and 76b wires at the exhaust port (Figure 16). Also notable is the reduction in the peak-peak measured temperature fluctuation of the 76 µm wires at the exhaust manifold (Figure 18) when compared to the exhaust port (Figure 16) at SS1. In Figure 18, the region between 180 CAD and 360 CAD shows

FIGURE 16 Mean ± 2σ and 300 cycle-averaged temperature signals of Taut1-v1 at SS1 and placed at the exhaust port centerline.

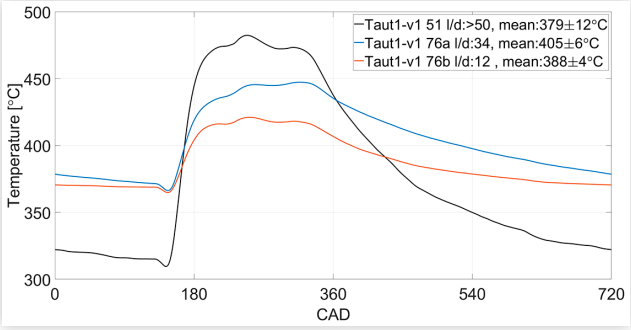

FIGURE 17 Slack and taut sensors tested at the exhaust manifold.

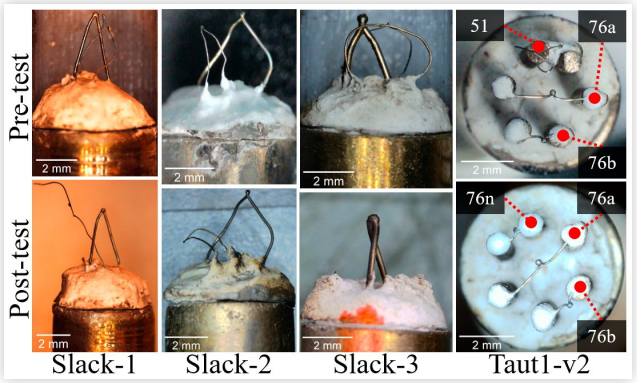

FIGURE 18 Mean ± 2σ and 300 cycle-averaged temperature signals of Taut1-v2 at SS1 and placed in the exhaust manifold (Eman-2).

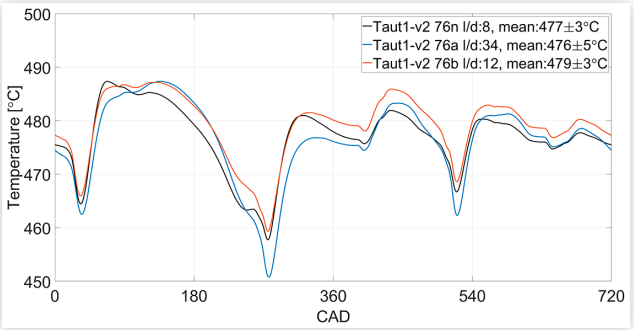

the maximum instantaneous difference of 7–9 °C between the longest 76a wire and the shorter 76b and 76n wires. The temperature dip between 180 CAD and 360 CAD corresponds to the missing exhaust pulse of Cylinder-6 in the exhaust manifold. The mean temperature and the cycle-to-cycle mean temperature variation (±2σ) among the Taut1-v2 wires are also comparable and within 2–3 °C at SS1. While the mean temperature does not show a trend with the wire l/d, the cycle-to-cycle mean temperature variation is marginally higher for the longest 76a wire.

The mean temperature observations in Figure 18 are similar to those made with the Slack-1 51 µm wires at the measurement section (Figure 10) which points to a greater significance of exhaust flow–related effects at this exhaust condition. However, the sensitivities of a l/d reduction on the instantaneous measured temperature and the cycle-to-cycle mean temperature variation is noticeable and in agreement with observations at the exhaust port (76a and 76b in Figure 16) and Slack-1 51 wires at the measurement section (Figure 10).

Summary and Conclusions

Sensor design parameters of thin-wire thermocouples, including the wire diameter, the wire length-to-diameter ratio (l/d), and the mounting of wires as slack (unsupported and without pretension) and taut (supported with pretension) are consequential to both sensor robustness and response. These sensor design parameters were experimentally evaluated in the exhaust of a heavy-duty diesel engine to determine a robust thin-wire thermocouple design and improved accuracy for EGT measurements. Wide-ranging exhaust conditions were tested by varying the engine operating points and measurement locations.

From the perspective of sensor robustness, the 76 µm taut wires with ceramic-coated weld faces endured over 3 h of engine operation without wire deformation or failure. Similar robustness was exhibited by slack design sensors with larger wire diameters (127 µm and 254 µm) and reduced exposed wire length (l/d) thinner wires (51 µm and 76 µm) only at a flow-conditioned measurement location. The experiments show that

- The taut wire design with coated weld faces is insensitive to the tested exhaust conditions and represents a robust thin-wire thermocouple sensor design.
- The slack wire design is sensitive to both sensor design parameters and the exhaust flow conditions that restrict its application.
- Type-K thin-wire thermocouple drift is insignificant under the tested conditions and durations irrespective of the sensor design parameters and minimizes the requirement for periodic calibrations.

From the perspective of sensor response, the accuracy of both the cycle-resolved and mean-measured EGT can be improved significantly by lowering the wire diameter while also increasing the exposed wire length, i.e., increasing the l/d. These sensor design changes also improve the measured sensitivity to cycle-to-cycle variations in the mean EGT. The mean EGT sensitivity alone was not generalizable with respect to the sensor design parameters in instances where the significance of exhaust flow conditions is considered dominant.

The results indicate that thin-wire thermocouples with smaller wire diameters and longer exposed lengths (a higher l/d), when placed taut with coated weld faces, improve their robustness to response tradeoff, enabling more accurate EGT measurements over longer test durations in ICEs.

Acknowledgments

The authors acknowledge Ted Holmberg (Scania CV AB) for designing the single-pipe exhaust setup and helping prepare the data acquisition system. Tomas Östberg (KTH) is acknowledged for support with setup fabrication and installation. Jan Stamer (KTH), Jonas Vikström (KTH), and Mattias Forsblom (KTH) are acknowledged for assisting in setup fabrication. Seshagopalan Thorapalli Muralidharan (KTH) is acknowledged for designing and assembling the custom thermocouple amplifier boards. Leif Pettersson (KTH) is acknowledged for providing access to the micro-arc welder used for preliminary sensor fabrication trials. Dr. Ramis Örlü (KTH) and Yushi Murai (KTH) are thanked for their valuable inputs and guidance concerning the design and fabrication of thermal anemometers. Beichuan Hong (KTH) is acknowledged for supporting the execution of experimental activities and aiding in data visualization. Anton Boström (KTH) and Christer Löfgren (KTH) are thanked for lab management and purchasing. Andreas Lius (KTH) is acknowledged for preparing a Labview-based data logging interface to depth profile the thermocouple calibrator. Haldenwanger GmbH is acknowledged for supplying the ceramic rod samples used in this study.

The Competence Center for Gas Exchange (CCGEx) and the Swedish Energy Agency (Energimyndigheten) are acknowledged for financing this study.

Contact Information

Varun Venkataraman
Doctoral Student
KTH Royal Institute of Technology
CCGEx Engineering Design/Mechatronics
Brinellvägen 83
SE-100 44 Stockholm, Sweden
varunve@kth.se

Abbreviations

ADC - Analog-to-digital converter
ASTM - American Society for Testing and Materials
ATDCf - After firing top dead center
AWG - American wire gauge
B0 - 0% biodiesel/neat diesel
BMEP - Brake mean effective pressure
CAC - Charge air cooler
CAD - Crank angle degree
DAQ - Data acquisition
EAT - Exhaust aftertreatment
ECU - Electronic control unit
EGT - Exhaust gas temperature
Eman-x - Sensor location in the exhaust manifold, x = 1–2
FEP - Fluorinated ethylene propylene
FS - Full scale
ICE - Internal combustion engine
IEC - International electrotechnical commission
IMEP - Indicated mean effective pressure
LSx - Load sweep test points, x = 1–4
MIMS - Mineral insulated metal sheathed
RWT - Resistance wire thermometers
SSx - Speed sweep test points, x = 1–4
VGT - Variable geometry turbine

Symbols

2σ - Two standard deviations
d - Thin-wire thermocouple wire diameter
l/d - Wire length-to-diameter ratio
L/D - Pipe length-to-diameter ratio

References

1. Gamma Technologies, "GT-SUITE Engine Performance Application Manual," 2019.
2. Ehrlich, D.A., "Characterization of Unsteady On-Engine Turbocharger Turbine Performance," Purdue University, West Lafayette, IN, 1998, ISBN:9780599406865.
3. Mollenhauer, K., "Measurement of Instantaneous Gas Temperatures for Determination of the Exhaust Gas Energy of a Supercharged Diesel Engine," SAE Technical Paper 670929, 1967, doi:https://doi.org/10.4271/670929.
4. Caton, J.A. and Heywood, J.B., "An Experimental and Analytical Study of Heat Transfer in an Engine Exhaust Port," *Int. J. Heat Mass Transf.* 24, no. 4 (1981): 581-595, doi:10.1016/0017-9310(81)90003-X.
5. Benson, R.S. and Galloway, K., "An Experimental and Analytical Investigation of the Gas Exchange Process in a Multi-Cylinder Pressure-Charged Two-Stroke Engine," *J. Appl. Mech. Trans. ASME* 183, no. 1 (1968): 253-279, doi:10.1115/1.4012178.
6. Chomiak, J. and Niedzialek, B., "Measurement of Rapidly Varying Gas Temperatures in an Unsteady Flow," *Int. J. Heat Mass Transf.* 10, no. 11 (1967): 1571-1579, doi:10.1016/0017-9310(67)90008-7.
7. Childs, P.R.N., Greenwood, J.R., and Long, C.A., "Review of Temperature Measurement," *Rev. Sci. Instrum.* 71, no. 8 (2000): 2959-2978, doi:10.1063/1.1305516.
8. Zhao, H. and Ladommatos, N., "In-Cylinder Gas Temperature Measurement," in *Engine Combustion Instrumentation and Diagnostics* (Warrendale, PA: SAE International, 2001), 640, ISBN:978-0-7680-0665-0.
9. Olczyk, A., "Problems of Unsteady Temperature Measurements in a Pulsating Flow of Gas," *Meas. Sci. Technol.* 19, no. 5 (2008): 055402, doi:10.1088/0957-0233/19/5/055402.
10. Benson, R.S. and Brundrett, G.W., "Development of a Resistance Wire Thermometer for Measuring Transient Temperatures in Exhaust Systems of Internal Combustion Engines," *Temp.: Its Meas. Control Sci. Ind.* 3, no. 2 (1962): 631-653.
11. Caton, J., "Comparisons of Thermocouple, Time-Averaged and Mass-Averaged Exhaust Gas Temperatures for a Spark-Ignited Engine," SAE Technical Paper 820050, 1982, doi:https://doi.org/10.4271/820050.
12. Kee, R., O'Reilly, P., Fleck, R., and McEntee, P., "Measurement of Exhaust Gas Temperatures in a High Performance Two-Stroke Engine," SAE Technical Paper 983072, 1998, doi:https://doi.org/10.4271/983072.
13. Tagawa, M. and Ohta, Y., "Two-Thermocouple Probe for Fluctuating Temperature Measurement in Combustion—Rational Estimation of Mean and Fluctuating Time Constants," *Combust. Flame* 109, no. 4 (1997): 549-560, doi:10.1016/S0010-2180(97)00044-8.
14. Lowell, H.H., *Design and Applications of Hot-Wire Anemometers for Steady-State Measurements at Transonic and Supersonic Airspeeds* (Washington, DC: National Advisory Committee for Aeronautics, 1950)
15. Perry, A.E., "The Aeroelastic Behaviour of Hot-Wire Anemometer Filaments in an Air Stream," in *Hot-Wire Anemometry* (New York, USA: Oxford University Press, 1982), 93-97.
16. Kee, R., Hung, P., Fleck, B., Irwin, G. et al., "Fast Response Exhaust Gas Temperature Measurement in IC Engines

Robert," SAE Technical Paper 2006-01-1319, 2006, doi:https://doi.org/10.4271/2006-01-1319.

17. Kar, K., Roberts, S., Stone, R., Oldfield, M. et al., "Instantaneous Exhaust Temperature Measurements Using Thermocouple Compensation Techniques," SAE Technical Paper 2004-01-1418, 2004, doi:https://doi.org/10.4271/2004-01-1418.
18. Kar, K., Swain, A., Raine, R., Roberts, S. et al., "Cycle-by-Cycle Variations in Exhaust Temperatures Using Thermocouple Compensation Techniques," SAE Technical Paper 2006-01-1197, 2006, doi:https://doi.org/10.4271/2006-01-1197.
19. Morey, F. and Seers, P., "Comparison of Cycle-by-Cycle Variation of Measured Exhaust-Gas Temperature and In-Cylinder Pressure Measurements," *Appl. Therm. Eng.* 30, no. 5 (2010): 487-491, doi:10.1016/j.applthermaleng.2009.10.011.
20. Papaioannou, N., Leach, F., and Davy, M., "Effect of Thermocouple Size on the Measurement of Exhaust Gas Temperature in Internal Combustion Engines," SAE Technical Paper 2018-01-1765, 2018, doi:https://doi.org/10.4271/2018-01-1765.
21. Gardiner, D.P., "Misfire Detection for Spark Ignition Engines Based upon Cycle-by-Cycle Exhaust Temperature Sensing," in *Proceedings of the ASME Internal Combustion Engine Division 2010 Fall Technical Conference Proceedings of the ASME 2010 Internal Combustion Engine Division Fall Technical Conference, ICEF2010*, San Antonio, TX, September 12-15, 2010, ASME, 697-706, doi:https://doi.org/10.1115/ICEF2010-35153.
22. Gardiner, D.P., Neill, W.S., and Chippior, W.L., "Real-Time Monitoring of Combustion Instability in a Homogeneous Charge Compression Ignition (HCCI) Engine Using Cycle-by-Cycle Exhaust Temperature Measurements," in *ASME 2012 Internal Combustion Engine Division Fall Technical Conference, ICEF 2012*, Vancouver, BC, Canada, 2012, 657-666, doi:10.1115/ICEF2012-92191.
23. ECM, "FastTEMP Fast Response Thermocouple Module," February 2023, accessed 02 Feburay 2023, https://ecm-co.com/product/fasttemp-kit/.
24. Mirhashemi, A., Szczudlak, J.D., and Morris, S.C., "Hot-Wire Probe Design and Calibration for High-Speed, High-Temperature Flows," *Meas. Sci. Technol.* 32, no. 4 (2021): 044002, doi:10.1088/1361-6501/abcefc.
25. Venkataraman, V., Murai, Y., Liverts, M., Örlü, R. et al., "Resistance Wire Thermometers for Temperature Pulse Measurements on Internal Combustion Engines," in *SMSI2020—Sensor and Measurement Science International* (AMA Service GmbH, Wunstorf, Germany, 2020), 252-253, doi:10.5162/SMSI2020/P2.14.
26. Bradley, D. and Matthews, K.J., "Measurement of High Gas Temperatures with Fine Wire Thermocouples," *J. Mech. Eng. Sci.* 10, no. 4 (1968): 299-305, doi:https://doi.org/10.1243/JMES_JOUR_1968_010_048_02.
27. Whitaker, S., "Forced Convection Heat Transfer Correlations for Flow in Pipes, Past Flat Plates, Single Cylinders, Single Spheres, and for Flow in Packed Beds and Tube Bundles," *AIChE J.* 18, no. 2 (1972): 361-371, doi:10.1002/aic.690180219.
28. Bergman, T.L., Lavine, A.S., Incropera, F.P., and Dewitt, D.P., "Chapter 8: Internal Flow," in *Introduction to Heat Transfer*, 6th ed. (John Wiley & Sons, Inc., Hoboken, NJ, USA), 2011, 491.
29. Lienhard, J.H. IV and Lienhard, J.H. V, "Chapter 7: Forced Convection in a Variety of Configurations," in *A Heat Transfer Textbook, 2.12* (Cambridge, MA: Phlogiston Press, 2018), 356-358.
30. Analog Devices, "Thermocouple Conditioner and Setpoint Controller AD596/AD597," October 2022, accessed 13 October 2022, https://www.analog.com/media/en/technical-documentation/data-sheets/AD596_597.pdf.
31. Muñoz, A., Blu, T., and Unser, M., "Least-Squares Image Resizing Using Finite Differences," *IEEE Trans. Image Process* 10, no. 9 (2001): 1365-1378, doi:https://doi.org/10.1109/83.941860.
32. Schafer, R.W., "What Is a Savitzky-Golay Filter?" *Signal Process. Mag.* 28, no. 4 (2011): 111-117, doi:10.1109/MSP.2011.941097.

Appendix A

Controlled Engine Boundary Conditions

FIGURE A.1 Single-pipe (Cylinder-6) backpressure (mean ± 2σ) over the engine operating points.

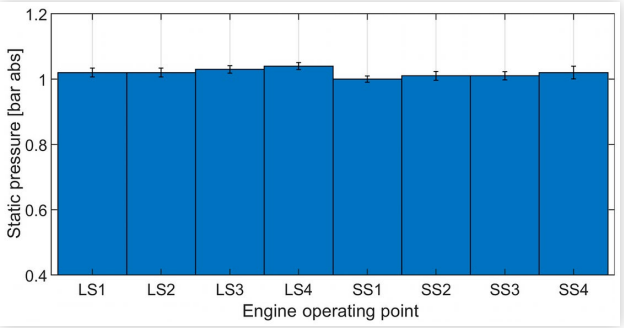

Single-Pipe (Cylinder-6) Exhaust Gas Mass Flow Estimation

The single-pipe exhaust of Cylinder-6 did not have a dedicated exhaust flowmeter. Hence, an indirect estimation of the exhaust gas mass flow was performed using readings from the fuel flow measurements of the fuel scale in Table 3 and lambda estimates from a Horiba MEXA-7100DEGR. Time-averaged readings from the Horiba analyzer were obtained at 2 Hz over 2 min in conjunction with the slow experimental data logs in preparatory tests that were used to identify the desired engine operating points shared in the study. The total fuel flow was scaled down to one cylinder, assuming equal fuel distribution across cylinders. The Horiba analyzer used

TABLE A.1 Single-pipe exhaust mass flow estimates over the speed sweep points.

Operating point	Speed [rpm]	Lambda Cylinder-6, Horiba no O_2 [-]	Total fuel flow, AVL 733s [g/s]	Single-pipe exhaust gas mass flow estimate [g/s]	Single-pipe engine speed normalized exhaust gas flow estimate [g/cyc]
SS-1	700	1.99	3.15	15.70	2.69
SS-2	1100	2.05	4.65	23.81	2.60
SS-3	1500	2.27	5.62	31.74	2.54
SS-4	1900	2.50	6.70	41.59	2.63

the no O_2 method for single-pipe lambda estimation based on raw emission readings. Lambda estimates from a Bosch LSU 4.9 lambda sensor in the single pipe were noticeably affected by the strong pressure fluctuations and hence avoided. The estimated exhaust gas mass flow was normalized by the engine speed to determine a speed-normalized exhaust mass flow to be indicative of the trapped mass in Cylinder-6 with the intention of providing comparable in-cylinder pressure conditions at the exhaust valve opening.

Thin-Wire Thermocouple Linearity and Static Calibration Functions

Figure A.2 depicts the pre-test linearity of all thin-wire thermocouples. The Taut1-v2 sensor was the exception with two wires that had test exposure before the 1st static calibration and were used as Taut1-v1 (refer to sensor Taut1-v1 and Taut1-v2 in Table A.4).

FIGURE A.2 Consolidated linearity check of all wires from all tested sensors wherein the data points are lumped at the sensor level. The dashed line indicates the base scaling of the amplifier at 10 mV/°C.

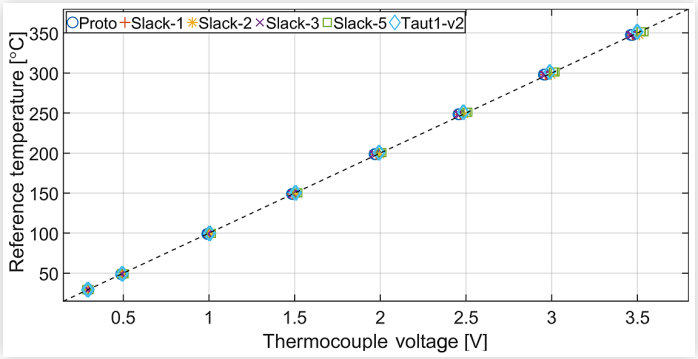

TABLE A.2 Static calibration linear fit functions for all thin-wire thermocouple sensor data analyzed in this study.

Sensor label	Wire diameter [μm]	Calibration function	R^2
Proto	127	T = 100.77 V −0.81	>0.99
Slack-1	51a	T = 100.62 V −0.78	>0.99
	51b	T = 100.41 V −0.63	>0.99
	127	T = 100.70 V −0.75	>0.99
Slack-3	51	T = 100.77 V −0.89	>0.99
	76	T = 100.94 V −0.26	>0.99
	254	T = 101.17 V −0.99	>0.99
Taut1-v2	76n	T = 100.82 V −1.04	>0.99
	76a	T = 100.72 V −0.01	>0.99
	76b	T = 100.75 V −0.78	>0.99

Slack and Taut Sensor Operational Summary

TABLE A.3 Detailed test and operational summary of slack design sensors.

Sensor label/Wire diameters [μm]	Sensor test and calibration sequence				Operational summary
Proto 51-127-76 butt weld	**Test/Calibration**	**Measurement location**	**Duration [min]**	**Functional wires**	The 51 μm wire failed after 1 h at the measurement section at LS2 upon the second trial. Static calibration cycles: 3
	Pre-test calibration	Not applicable	Not applicable	3	
	LS2	Measurement section	60	3	The 76 μm wire failed after 2 h at the measurement section at LS2 and 10 min at the single-pipe exhaust port (upper) during warm-up
	Post-test calibration-1	Not applicable	Not applicable	3	
	Post-test calibration-2	Not applicable	Not applicable	3	The 127 μm wire failed after 2 h at the measurement section at LS2 and 1 h and 36 min at the single-pipe exhaust port (upper) from warm-up through the speed sweep test points
	LS2	Measurement section	60	2,51 μm failed	
	Post-test calibration-3	Not applicable	Not applicable	2	Static calibration cycles for 76 μm and 127 μm wires: 4
	Warm-up + SS1-4 + LS3-4	Port (upper)	30 + 66	1,76 μm failed	
Slack-1 51-127-51	Pre-test calibration	Not applicable	Not applicable	3	The 1st 51 μm wire failed after ~1.5 h at the measurement section at the highest load point of the load sweep (LS4)
	LS1-4	Measurement section	90	3,1×51 μm failed	
	Post-test calibration-1	Not applicable	Not applicable	2	The second 51 μm wire failed after 2 h 40 min at the measurement section (survived the full test matrix) and failed after 10 min in the exhaust manifold (Eman-1) at LS1
	SS1-4	Measurement section	70	2	
	Post-test calibration-2	Not applicable	Not applicable	2	The 127 μm wire survived 2 h 40 min at the measurement section, 10 min at the exhaust manifold (Eman-1) at LS1, and an additional 2 h at the port (centerline). The wire essentially survived the entire test matrix over the measurement section and the port
	LS1	Exhaust manifold (Eman-1)	10	1, second 51 μm failed	
	Full test matrix	Port (centerline)	120	1	Static calibration cycles for all wires: 3
Slack-2 51-127	Pre-test calibration	Not applicable	Not applicable	1	The 51 μm wire failed after ~0.5 h at the exhaust manifold (Eman-2) after successfully surviving 1 warm-up cycle and some exposure at SS1
	Warm-up cycle + SS1	Exhaust manifold (Eman-2)	25 + 5	1	
	Warm-up cycle	Exhaust manifold (Eman-2)	5	0,51 μm failed	Static calibration cycles: 1
Slack-3 51-254-76 butt weld	Pre-test calibration	Not applicable	Not applicable	3	All wires survived the entire test matrix at the measurement section with a total test duration of 2 h 40 min
	LS1-4	Measurement section	77	3	
	SS1-4	Measurement section	83	3	At the exhaust manifold (Eman-2), the 51 μm wire failed first after 13 min of operation at LS1
	Post-test calibration-1	Not applicable	Not applicable	3	
	LS1	Exhaust manifold (Eman-2)	13	2,51 μm failed	The 76 μm wire failed after an additional 20 min (total ~0.5 h exposure) of testing at LS2. The 254 μm wire endured over 3 h and 13 min of testing and did not fail.
	LS2	Exhaust manifold (Eman-2)	20	1,76 μm failed	
					Static calibration cycles for all wires: 2
Slack-5 127-51-254	Pre-test calibration	Not applicable	Not applicable	3	All wires survived the tests at the measurement section for 1 h 20 min.
	5-point test:	Measurement section	80	3	
	SS1-3 + LS3-4				The 51 μm wire failed after 35 min of tests at the port (centerline) at SS2 while the 127 and 254 μm wires survived the entire test at the port (centerline) enduring a cumulative test time of 2 h 25 min.
	SS1-4	Port (centerline)	65	2,51 μm failed	
	Post-test calibration-1	Not applicable	Not applicable	2,51 μm failed	Static calibration cycles: 1 (51 μm) and 2 (127–254 μm)

TABLE A.4 Detailed test and operational summary of taut design sensors.

Sensor label/Wire diameters [μm]	Sensor test and calibration sequence				Operational summary
Taut-1 (v1) 51-76a-76b	**Test/Calibration**	**Measurement location**	**Duration [min]**	**Functional wires**	The 51 μm slack welded wire failed after 1 h at the exhaust port (centerline) at SS4 and was replaced by a 76 μm bead welded wire.
Taut-1 (v2) 76n-76a-76b	Taut1 (v1): SS1-2 + LS3-4 + SS4	Port (centerline)	60	2,51 μm failed	
	Post-test calibration-1	Not applicable	Not applicable	3,76 μm replaced 51 μm	The 76 μm wires survived all test points at the port (centerline) and exhaust manifold (Eman-2) for a total test duration of 3 h and 40 min [2 h 40 min for the new 76 μm wire (76n) in Taut1 (v2)].
	Taut1 (v2): Warm-up cycle + LS1 + full test matrix	Exhaust manifold (Eman-2)	30 + 10 + 120	3	
	Post-test calibration-2	Not applicable	Not applicable	3	Static calibration cycles for all 76 μm wires: 2
					The Taut1 (v1) configuration was not calibrated before the 1st experiment which was performed at the exhaust port centerline